

Covert Millimeter-Wave Communication: Design Strategies and Performance Analysis

Mohammad Vahid Jamali and Hessam Mahdaviifar, *Member, IEEE*

Abstract—In this paper, we investigate covert communication over millimeter-wave (mmWave) frequencies. In particular, a mmWave transmitter, referred to as Alice, attempts to reliably communicate to a receiver, referred to as Bob, while hiding the existence of communication from a warden, referred to as Willie. In this regard, operating over mmWave bands not only increases the covertness thanks to directional beams, but also increases the transmission data rates given much more available bandwidths and enables ultra-low form factor transceivers due to the lower wavelengths used compared to the conventional radio frequency (RF) counterpart. We first assume that the transmitter Alice employs two independent antenna arrays in which one of the arrays is to form a directive beam for data transmission to Bob. The other antenna array is used by Alice to generate another beam toward Willie as a jamming signal while changing the transmit power independently across the transmission blocks in order to achieve desired covertness. For this dual-beam setup, we characterize Willie’s detection error rate with the optimal detector and the closed-form of its expected value from Alice’s perspective. We then derive the closed-form expression for the outage probability of the Alice-Bob link, which enables characterizing the optimal covert rate that can be achieved using the proposed setup. We further obtain tractable forms for the ergodic capacity of the Alice-Bob link involving only one-dimensional integrals that can be computed in closed forms for most ranges of the channel parameters. Finally, we highlight how the results can be extended to more practical scenarios, particularly to cases where perfect information about the location of the passive warden is not available. Our results demonstrate the advantages of covert mmWave communication compared to the RF counterpart. The research in this paper is the first analytical attempt in exploring covert communication using mmWave systems.

Index Terms—Covert communication, mmWave communication, communication with low probability of detection, detection error rate, effective covert rate, ergodic capacity, Nakagami fading channels.

I. INTRODUCTION

Rapid growth of wireless networks and the emergence of variety of applications, including the Internet of Things (IoT), massive machine-type communication (mMTC), and critical controls, necessitate sophisticated solutions to secure data transmission. Traditionally, the main objective of security schemes, using either cryptographic or information-theoretic approaches, is to secure data in the presence of adversary

eavesdroppers. However, a stronger level of security can be obtained in wireless networks if the existence of communication is hidden from the adversaries. To this end, recently, there has been increasing attention to investigate covert communication, also referred to as communication with *low probability of detection* (LPD), in various scenarios with the goal of hiding the existence of communication [2]–[9]. Generally speaking, covert communication refers to the problem of reliable communication between a transmitter Alice and a receiver Bob while maintaining a low probability of detecting the existence of communication from the perspective of a warden Willie [3].

The information-theoretic limits on the rate of covert communication have been presented in [2] for additive white Gaussian noise (AWGN) channels, where it is proved that $\mathcal{O}(\sqrt{n})$ bits of information can be transmitted to Bob, reliably and covertly, in n uses of the channel, as $n \rightarrow \infty$. The same square root law has been developed for binary symmetric channels (BSCs) in [4] and discrete memoryless channels (DMCs) in [5]. Moreover, the principle of channel resolvability has been used in [6] to develop a coding scheme that can reduce the number of required shared key bits. Also, the first- and second-order asymptotics of covert communication over binary-input DMCs are studied in [7]. The covert communication setup is also extended to broadcast channels [8] and to multiple-access channels [9] from an information-theoretic perspective.

The achievable covert rate in the aforementioned framework is zero as n grows large since $\lim_{n \rightarrow \infty} \mathcal{O}(\sqrt{n})/n = 0$. However, it is demonstrated that positive covert rates can be achieved by introducing additional uncertainty, from Willie’s perspective, into the system. For instance, it is shown in [10], [11] that Willie’s uncertainty about his noise power helps achieving positive covert rates. Moreover, by considering slotted AWGN channels, it is proved in [12] that positive covert rates are achievable if the warden does not know when the transmission is taking place. The possibility of achieving positive-rate covert communication is further demonstrated for several other scenarios such as amplify-and-forward (AF) relaying networks with a greedy relay attempting to transmit its own information to the destination on top of forwarding the source’s information [13], dual-hop relaying systems with channel uncertainty [14], a downlink scenario under channel uncertainty and with a legitimate user as cover [15], and a single-hop setup with a full-duplex receiver acting as a jammer [16]. Additionally, covert communication in the presence of a multi-antenna adversary, under delay constraints, and for the case of quasi-static wireless fading channels is considered in [17]. In [18], channel inversion power control is adopted to achieve covert communication with the aid of a full-duplex receiver. Covert communications in the context of unmanned

The material in this paper was presented in part at the IEEE Global Communications Conference (GLOBECOM), Waikoloa, HI, USA, Dec. 2019 [1].

The authors are with the Department of Electrical Engineering and Computer Science, University of Michigan, Ann Arbor, MI 48109, USA (e-mail: mvjamali@umich.edu, hessam@umich.edu).

This work was supported by the National Science Foundation under grants CCF-1763348, CCF-1909771, and CCF-1941633.

aerial vehicle (UAV) networks is considered in [19]. Very recently, the problem of joint covert communication and secure transmission in untrusted relaying networks in the presence of multiple wardens has been considered in [20]. Moreover, the benefits of beamforming in improving the performance of covert communication in the presence of a jammer has been studied in [21].

Prior studies on covert communication in wireless networks mostly consider omnidirectional transmission over conventional radio frequency (RF) wireless links. However, a superior performance can be potentially attained when performing the covert communication over millimeter-wave (mmWave) bands. In particular, operating over mmWave bands not only increases the covertness thanks to directional beams, but also increases the transmission data rates given much more available bandwidths and enables ultra-low form factor transceivers due to the lower wavelengths used compared to the conventional RF counterpart. This makes the mmWave band a suitable option for covert communication to increase the security level of wireless applications involving critical data. Also, with the advancement in mmWave communications and rapid development of mmWave cellular networks in the fifth generation of wireless networks (5G), mmWave systems will serve as major components for a wide range of emerging wireless networking applications and use cases. This necessitates secure transmission schemes for mmWave systems and further highlights the importance of covert mmWave communication.

The channel model and system architecture of mmWave communication systems significantly differ from those of RF communication. In particular, communication over mmWave bands can exploit directive beams, thanks to the deployment of massive antenna arrays, to compensate for the significant path loss over this range of frequency. Meanwhile, the significant susceptibility of directive mmWave links to blockage results in a nearly bimodal channel depending on whether a line-of-sight (LOS) link exists between the transmitter and receiver [22]. Furthermore, the properties of mmWave and RF channels, including path loss and statistical distribution of fading, are often modeled very differently. Therefore, the existing results on covert communication cannot immediately be extended to covert communication over mmWave bands.

In this paper, we study covert communication over mmWave channels from a communication theory perspective. More specifically, we analyze the performance of the system in the limit as the block-length n grows large. In order to achieve a positive-rate covert communication, the transmitter Alice is equipped with two antenna arrays each pointed to a different direction and carrying independent data streams. The first antenna array forms a directive beam for covert data transmission to Bob. The second array is used to generate another beam toward Willie as a jamming signal while the transmit power is changed independently across transmission blocks in order to achieve desired covertness. For this dual-beam transmitter setup we characterize Willie's optimal detection performance in terms of the overall detection error, and derive the closed form for the expected value of the detection error rate from Alice's perspective. We then obtain the closed-form expression for the outage probability of the Alice-Bob link.

This leads to characterization of the optimal covert rate that is achieved in our proposed setup. We further obtain tractable forms for the ergodic capacity of the Alice-Bob link involving only one-dimensional integrals that can be computed in closed forms for most ranges of the channel parameters. Finally, we highlight how the results can be extended to more practical scenarios, particularly to the cases where perfect information about Willie's location is not available to Alice. Our results highlight the advantages of covert mmWave communication compared to the RF counterpart.

The research in this paper is the first attempt in analytical studies of covert communication over mmWave systems. It is worth mentioning that a conceptual framework for covert mmWave communication was envisioned in [23] without providing analytical studies. To the best of authors' knowledge, no analytical characterization for covert mmWave system has been carried out in prior works. Very recently, after the appearance of the initial version of this work [1], Zhang *et al.* [24] studied joint beam training and data transmission for covert mmWave communication. More specifically, the authors of [24] aimed at jointly optimizing the beam training duration (to establish a directional link between Alice and Bob), training power, and data transmission power to maximize the effective covert rate while satisfying the covertness constraint on Willie.

The rest of the paper is organized as follows. In Section II, we briefly summarize the mmWave channel model and describe the proposed covert mmWave communication setup. In Section III, we analyze Willie's overall error rate with an optimal radiometer detector, and then obtain its expected value from Alice's perspective. Section IV is devoted to studying the performance of the Alice-Bob link, in terms of outage probability, effective covert rate, and ergodic capacity. Discussions about various realistic scenarios, including imperfect knowledge about Willie's location, as well as some future research directions are provided in Section V. Finally, extensive numerical results are presented in Section VI, and the paper is concluded in Section VII.

II. CHANNEL AND SYSTEM MODELS

A. Channel Model

Recent experimental studies have demonstrated that mmWave links are highly sensitive to blocking effects [22], [25]. In order to model this characteristic, a proper channel model should differentiate between the LOS and non-LOS (NLOS) channel models since the path loss in the NLOS links can be much higher than that of the LOS path due to the weak diffractions in the mmWave band. Therefore, two different sets of parameters are considered for the LOS and NLOS mmWave links, and a deterministic function $P_{\text{LOS}}(d_{ij}) \in [0, 1]$, that is a non-increasing function of the link length d_{ij} (in meters) between the nodes i and j , is defined to characterize the probability of an arbitrary link of length d_{ij} being LOS. Detailed overview of several blocking models for characterizing $P_{\text{LOS}}(d_{ij})$ is provided in [22]. In this paper, we consider a generic function $P_{\text{LOS}}(d_{ij})$ throughout our analysis and use the model $P_{\text{LOS}}(d_{ij}) = e^{-d_{ij}/200}$, suggested in [22], for our numerical analysis.

TABLE I
PROBABILITY MASS FUNCTION (PMF) OF THE DIRECTIVITY GAIN OF A
NODE q WITH BEAMSTEERING ERROR [26].

k	1	2
$g_k^{(q)}$	$M_{\mathcal{X}}^{(q)}$	$m_{\mathcal{X}}^{(q)}$
$b_k^{(q)}$	$F_{ \mathcal{E}_{\mathcal{X}}^{(q)} }(\theta_{\mathcal{X}}^{(q)}/2)$	$1 - F_{ \mathcal{E}_{\mathcal{X}}^{(q)} }(\theta_{\mathcal{X}}^{(q)}/2)$

In the following, we describe how the channel for LOS and NLOS links can be characterized. Same as in [22], we express the channel coefficient for an arbitrary mmWave link between the transmitter i and receiver j as $h_{ij} = \tilde{h}_{ij} \sqrt{G_{ij} L_{ij}}$, where \tilde{h}_{ij} , G_{ij} , and L_{ij} are the channel fading coefficient, the total directivity gain (including both the transmitter and the receiver beamforming gains), and the path loss of the i - j mmWave link, respectively.

To characterize the path loss L_{ij} of the i - j link with the length d_{ij} , we consider different path loss exponents (α_L, α_N) and intercepts (C_L, C_N) for the LOS and NLOS links, respectively. Let the path losses associated with the LOS and NLOS links be denoted by $L_{ij}^{(L)}$ and $L_{ij}^{(N)}$, respectively. Then the path loss L_{ij} is either equal to $L_{ij}^{(L)} = C_L d_{ij}^{-\alpha_L}$ with probability $P_{\text{LOS}}(d_{ij})$ or equal to $L_{ij}^{(N)} = C_N d_{ij}^{-\alpha_N}$ with probability $1 - P_{\text{LOS}}(d_{ij})$. Typical values for the path loss exponents and intercepts of the LOS and NLOS links can be found in the prior measurement works, e.g., [25].

To ascertain the total directivity gain G_{ij} , we use the common sectored-pattern antenna model adopted in [26], [27] which approximates the actual array beam pattern by a step function, i.e., with a constant main lobe gain $M_{\mathcal{X}}^{(q)}$ over the beamwidth $\theta_{\mathcal{X}}^{(q)}$ and a constant side lobe gain $m_{\mathcal{X}}^{(q)}$ otherwise, where $\mathcal{X} \in \{\text{TX}, \text{RX}\}$ and $q \in \{i, j\}$. Then, for a given link, if the spatial arrangement of the beams of the transmitter and receiver are known, the total directivity gain can be obtained from the product of the gains of the transmitter and receiver. If the main lobe of a node q (either transmitter or receiver) is pointed to another node, we assume that an additive beamsteering error exists, denoted by a symmetric random variable (RV) $\mathcal{E}_{\mathcal{X}}^{(q)}$, in the vicinity of the transmitter-receiver direction. Same as in [26], it is assumed that node q has a gain equal to $M_{\mathcal{X}}^{(q)}$ if $|\mathcal{E}_{\mathcal{X}}^{(q)}| < \theta_{\mathcal{X}}^{(q)}/2$, which occurs with probability $F_{|\mathcal{E}_{\mathcal{X}}^{(q)}|}(\theta_{\mathcal{X}}^{(q)}/2)$ with $F_X(x)$ being the cumulative distribution function (CDF) of the RV X . Otherwise, it has a gain equal to $m_{\mathcal{X}}^{(q)}$. Then the probability mass function (PMF) of the directivity gain of a node q with beamsteering error can be expressed as a RV taking the values $g_k^{(q)}$ with probabilities $b_k^{(q)}$, $k \in \{1, 2\}$, as summarized in Table I.

Finally, it is common in the literature to model the fading amplitude of mmWave links as independent Nakagami-distributed RVs with shape parameter $\nu \geq 1/2$ and scale parameter $\Omega = \mathbb{E}[|h_{ij}|^2] = 1$, and consider different Nakagami parameters for the LOS and NLOS links as ν_L and ν_N , respectively [22], [27]. In the case of Nakagami- m fading with parameters ν_B , $B \in \{L, N\}$, and $\Omega = 1$, $|h_{ij}|^2$ has a normalized gamma distribution with shape and scale parameters of ν_B and $1/\nu_B$, respectively. Therefore, the probability density

function (PDF) of $|\tilde{h}_{ij}|^2$ is given by [28]

$$f_{|\tilde{h}_{ij}|^2}(y) = \frac{\nu_B^{\nu_B} y^{\nu_B-1}}{\Gamma(\nu_B)} \exp(-\nu_B y). \quad (1)$$

Note that, from an information-theoretic perspective, mmWave communications, and in general wideband communications under power constraints, can be viewed as low-capacity scenarios [29]–[31] suggesting a natural framework for covert mmWave communication.

B. System Model

We consider a well-known setup for covert communication comprised of three parties: a transmitter Alice is intending to covertly communicate to a receiver Bob over mmWave bands when a warden Willie is attempting to realize the existence of this communication. Alice employs a dual-beam mmWave transmitter consisting of two antenna arrays. The first antenna array is used for the transmission to Bob while the second array is exploited as a jammer to enable positive-rate covert mmWave communication. Therefore, when Bob is not in the main lobe of the Alice-Willie link, he receives the jamming signal gained with the side lobe of the second array in addition to receiving the desired signal from Alice with the main lobe of the first array. Similarly, when Willie is not in the main lobe of the Alice-Bob link, he receives the desired signal gained with the side lobe of the first array in addition to receiving the jamming signal from Alice with the main lobe of the second array. On the other hand, when Bob is in the main lobe of the Alice-Willie link (or equivalently, Willie is in the main lobe of the Alice-Bob link), both of the received signals by Bob and Willie are gained with main lobes. Throughout our analysis in Sections III and IV, we assume that Alice, Bob, and Willie are in some fixed locations (hence, having some given directivity gains). And we leave the discussion about various realistic scenarios, such as imperfect knowledge of Willie's location, to Section V.

Let the channel coefficients between Alice's first and second arrays and the node $j \in \{b, w\}$ (representing Bob and Willie) be denoted by $h_{aj,f}$ and $h_{aj,s}$, respectively. Then it can be observed that the path loss gains are the same, i.e., $L_{aj,f} = L_{aj,s} \triangleq L_{aj}$, while the fading gains $|\tilde{h}_{aj,f}|^2$ and $|\tilde{h}_{aj,s}|^2$ are independent normalized gamma RVs. We assume quasi-static fading channels meaning that fading coefficients remain constant over a block of n channel uses. We further assume that Alice transmits the desired signal with a publicly-known power P_a while the jamming transmit power P_J of its second array is not known and is changed independently across transmission blocks. In this paper, we assume that P_J is drawn from a uniform distribution over the interval $[0, P_J^{\max}]$ while the results can be extended to other distributions using a similar approach. Let $G_{aj,f}$ and $G_{aj,s}$ denote the total directivity gains of the links between Alice's first and second arrays and the node $j \in \{b, w\}$, respectively. Then, the received signals by Bob and Willie at each channel use i ,

for $i = 1, 2, \dots, n$, is given by

$$\mathbf{y}_b(i) = \sqrt{P_a G_{ab,f} L_{ab}} \tilde{h}_{ab,f} \mathbf{x}_a(i) + \sqrt{P_J G_{ab,s} L_{ab}} \tilde{h}_{ab,s} \mathbf{x}_J(i) + \mathbf{n}_b(i), \quad (2)$$

$$\mathbf{y}_w(i) = \sqrt{P_a G_{aw,f} L_{aw}} \tilde{h}_{aw,f} \mathbf{x}_a(i) + \sqrt{P_J G_{aw,s} L_{aw}} \tilde{h}_{aw,s} \mathbf{x}_J(i) + \mathbf{n}_w(i), \quad (3)$$

respectively, where \mathbf{x}_a and \mathbf{x}_J are Alice's desired and jamming signals, respectively, each having a zero-mean Gaussian distribution satisfying $\mathbb{E}[|\mathbf{x}_a(i)|^2] = \mathbb{E}[|\mathbf{x}_J(i)|^2] = 1$. Moreover, \mathbf{n}_b and \mathbf{n}_w are zero-mean Gaussian noise components at Bob and Willie's receivers with variances σ_b^2 and σ_w^2 , respectively.

Finally, note that the results derived in this paper can be applied to a similar system model, though with Rayleigh fading channels, by substituting $\nu_B = 1$, since in the special case of $\nu_B = 1$ the normalized gamma distribution simplifies to the exponential distribution with mean one.

III. WILLIE'S DETECTION ERROR RATE

As discussed earlier, Willie's goal is to detect whether Alice is transmitting to Bob or not. It is assumed that Willie has a perfect knowledge about the channel between himself and Alice, and applies binary hypothesis testing while being unaware of the value of P_J . The null hypothesis \mathbb{H}_0 states that Alice did not transmit to Bob and the alternative hypothesis \mathbb{H}_1 specifies that a transmission from Alice to Bob occurred. Consequently, there are two types of errors that Willie can encounter specified as follows. First, Willie's decision of hypothesis \mathbb{H}_1 when \mathbb{H}_0 is true is referred to as a *false alarm* and its probability is denoted by P_{FA} . Second, Willie's decision in favor of \mathbb{H}_0 when \mathbb{H}_1 is true is referred to as a *missed detection* with the probability denoted by P_{MD} . Then Willie's overall detection error rate is defined as $P_{e,w} \triangleq P_{FA} + P_{MD}$. We say a positive-rate covert communication is possible if for any $\epsilon > 0$ there exists a positive-rate communication between Alice and Bob satisfying $P_{e,w} \geq 1 - \epsilon$ as the number of channel uses $n \rightarrow \infty$. In this section, we first obtain $P_{e,w}$ with assuming an optimal radiometer detector at Willie, and then derive the closed-form expression of the expected value of $P_{e,w}$ from Alice's perspective.

A. $P_{e,w}$ with the Optimal Detector at Willie

As it is proved in [32, Lemma 2] for AWGN channels and also pointed out in [15, Lemma 1], the optimal decision rule that minimizes Willie's detection error is given by

$$T_w \triangleq \frac{1}{n} \sum_{i=1}^n |\mathbf{y}_w(i)|^2 \underset{\mathbb{H}_0}{\overset{\mathbb{H}_1}{\geq}} \tau, \quad (4)$$

where τ is Willie's detection threshold for which we obtain the corresponding optimal value/range later in this subsection. Using (3) and the definition of T_w in (4), we can write T_w under hypotheses \mathbb{H}_0 , denoted by $T_w^{\mathbb{H}_0}$, as

$$T_w^{\mathbb{H}_0} = \left(P_J G_{aw,s} L_{aw} |\tilde{h}_{aw,s}|^2 + \sigma_w^2 \right) \frac{\chi_{2n}^2}{n}, \quad (5)$$

where χ_{2n}^2 denotes a chi-squared RV with $2n$ degrees of freedom. According to the strong law of large numbers $\frac{\chi_{2n}^2}{n}$

converges to 1, *almost surely*, as $n \rightarrow \infty$. Therefore, using Lebesgue's dominated convergence theorem [33], we can replace $\frac{\chi_{2n}^2}{n}$ by 1 to rewrite $T_w^{\mathbb{H}_0}$ as

$$T_w^{\mathbb{H}_0} = P_J G_{aw,s} L_{aw} |\tilde{h}_{aw,s}|^2 + \sigma_w^2. \quad (6)$$

Similarly, T_w under hypotheses \mathbb{H}_1 can be obtained as

$$T_w^{\mathbb{H}_1} = P_a G_{aw,f} L_{aw} |\tilde{h}_{aw,f}|^2 + P_J G_{aw,s} L_{aw} |\tilde{h}_{aw,s}|^2 + \sigma_w^2. \quad (7)$$

The optimal threshold of Willie's detector and its corresponding detection error are characterized in the following theorem.

Theorem 1. *The optimal threshold τ^* for Willie's detector is in the interval*

$$\tau^* \in \begin{cases} [\lambda_1, \lambda_2], & \lambda_1 < \lambda_2, \\ [\lambda_2, \lambda_1], & \lambda_1 \geq \lambda_2, \end{cases} \quad (8)$$

and the corresponding minimum detection error rate is

$$P_{e,w}^* = \begin{cases} 0, & \lambda_1 < \lambda_2, \\ 1 - \frac{P_a G_{aw,f} |\tilde{h}_{aw,f}|^2}{P_J^{\max} G_{aw,s} L_{aw} |\tilde{h}_{aw,s}|^2}, & \lambda_1 \geq \lambda_2, \end{cases} \quad (9)$$

where $\lambda_1 \triangleq P_J^{\max} G_{aw,s} L_{aw} |\tilde{h}_{aw,s}|^2 + \sigma_w^2$ and $\lambda_2 \triangleq P_a G_{aw,f} L_{aw} |\tilde{h}_{aw,f}|^2 + \sigma_w^2$.

Proof: Using (6), the false alarm probability is given by

$$P_{FA} = \Pr(T_w^{\mathbb{H}_0} > \tau) = \Pr\left(P_J > \frac{\tau - \sigma_w^2}{G_{aw,s} L_{aw} |\tilde{h}_{aw,s}|^2}\right) = \begin{cases} 1, & \tau < \sigma_w^2, \\ 1 - \frac{\tau - \sigma_w^2}{P_J^{\max} G_{aw,s} L_{aw} |\tilde{h}_{aw,s}|^2}, & \sigma_w^2 \leq \tau \leq \lambda_1, \\ 0, & \tau \geq \lambda_1. \end{cases} \quad (10)$$

Also, by (7) the missed detection probability is given by

$$P_{MD} = \Pr(T_w^{\mathbb{H}_1} < \tau) = \Pr\left(P_J < \frac{\tau - \lambda_2}{G_{aw,s} L_{aw} |\tilde{h}_{aw,s}|^2}\right) = \begin{cases} 0, & \tau < \lambda_2, \\ \frac{\tau - \lambda_2}{P_J^{\max} G_{aw,s} L_{aw} |\tilde{h}_{aw,s}|^2}, & \lambda_2 \leq \tau \leq \lambda_3, \\ 1, & \tau \geq \lambda_3, \end{cases} \quad (11)$$

where $\lambda_3 \triangleq \lambda_2 + P_J^{\max} G_{aw,s} L_{aw} |\tilde{h}_{aw,s}|^2$. Next, we consider the following two cases.

Case I: When $\lambda_1 < \lambda_2$, Willie's receiver can choose any thresholds in the interval $[\lambda_1, \lambda_2]$ to get both $P_{FA} = 0$ and $P_{MD} = 0$, resulting in zero detection error $P_{e,w} \triangleq P_{FA} + P_{MD}$.

Case II: When $\lambda_1 \geq \lambda_2$, we can write the overall detection error rate $P_{e,w} \triangleq P_{FA} + P_{MD}$, using (10) and (11), as

$$P_{e,w} = \begin{cases} 1, & \tau \leq \sigma_w^2, \\ 1 - \frac{\tau - \sigma_w^2}{P_J^{\max} G_{aw,s} L_{aw} |\tilde{h}_{aw,s}|^2}, & \sigma_w^2 \leq \tau \leq \lambda_2, \\ 1 - \frac{P_a G_{aw,f} |\tilde{h}_{aw,f}|^2}{P_J^{\max} G_{aw,s} L_{aw} |\tilde{h}_{aw,s}|^2}, & \lambda_2 \leq \tau \leq \lambda_1, \\ \frac{\tau - \lambda_2}{P_J^{\max} G_{aw,s} L_{aw} |\tilde{h}_{aw,s}|^2}, & \lambda_1 \leq \tau \leq \lambda_3, \\ 1, & \tau \geq \lambda_3. \end{cases} \quad (12)$$

Therefore, based on (12), the receiver never chooses $\tau \leq \sigma_w^2$ or $\tau \geq \lambda_3$ since they result in the worst performance $P_{e,w} = 1$. Moreover, (12) monotonically decreases, with respect to τ , in

the interval $\sigma_w^2 \leq \tau \leq \lambda_2$ until it reaches the constant value corresponding to $P_{e,w}$ in the interval $\lambda_2 \leq \tau \leq \lambda_1$, and then it monotonically increases in the interval $\lambda_1 \leq \tau \leq \lambda_3$ until it reaches 1. Therefore, the constant value of the detection error rate in the interval $\lambda_2 \leq \tau \leq \lambda_1$ is the minimum value of $P_{e,w}$ for $\lambda_1 \geq \lambda_2$ that can be attained using any threshold in the interval $[\lambda_2, \lambda_1]$. ■

Remark 1. Eq. (9) shows that for small values of P_J^{\max} with $P_J^{\max} G_{aw,s} |\tilde{h}_{aw,s}|^2 \leq P_a G_{aw,f} |\tilde{h}_{aw,f}|^2$ Willie can attain a zero error rate negating the possibility of achieving a positive-rate covert communication as $n \rightarrow \infty$. Although increasing P_J^{\max} beyond $P_a G_{aw,f} |\tilde{h}_{aw,f}|^2 / (G_{aw,s} |\tilde{h}_{aw,s}|^2)$ can increase $P_{e,w}^*$ and enable a positive-rate covert communication ($P_{e,w}^* \rightarrow 1$ as $P_J^{\max} \rightarrow \infty$), it also degrades the performance of the desired Alice-Bob link as we will see in Section IV. The superiority of covert mmWave communication to that of omni-directional RF communication becomes then apparent by observing the beneficial impact of beamforming. In fact, in the received signal by Willie, P_J is gained by $G_{aw,s}$ which is much larger than the gain $G_{aw,f}$ of P_a ; this simultaneously increases the jamming signal and decreases the desired signal received by Willie, i.e., significantly degrades the performance of Willie's detector. It will be shown in Section IV that an opposite situation happens for the Alice-Bob link where the desired signal is gained with $G_{ab,f}$ which is much larger than the gain $G_{ab,s}$ of the jamming signal.

B. $\mathbb{E}[P_{e,w}^*]$ From Alice's Perspective

Since Alice and Bob are unaware of the instantaneous realization of the channel between Alice and Willie, they should rely on the expected value of $P_{e,w}^*$. Note also that the minimum error rate $P_{e,w}^*$ in (9) is independent of the beamforming gain of Willie's receiver as it cancels out in the ratio of $G_{aw,f}/G_{aw,s}$ and also in the comparison between λ_1 and λ_2 . Furthermore, Alice perfectly knows the gain $m_{a,f}$ of the side lobe of her first array to Willie. However, she has uncertainty about the gain $g^{(a,s)}$ of the main lobe of the second array toward Willie due to the misalignment error; it is either $g_1^{(a,s)} \triangleq M_{a,s}$ with probability $b_1^{(a,s)} \triangleq F_{|\mathcal{E}_{a,s}|}(\theta_{a,s}/2)$ or $g_2^{(a,s)} \triangleq m_{a,s}$ with probability $b_2^{(a,s)} \triangleq 1 - F_{|\mathcal{E}_{a,s}|}(\theta_{a,s}/2)$. Moreover, Alice and Bob do not know whether the Alice-Willie link is LOS or NLOS; hence, they should take into account two possibilities given the LOS probability $P_{\text{LOS}}(d_{aw})$. In the following theorem, we characterize the expected value of $P_{e,w}^*$ from Alice's perspective in a closed form.

Theorem 2. *The expected value of $P_{e,w}^*$ from Alice's perspective is characterized as (13), shown at the bottom of this page, where $P_{aw}(\text{L}) \triangleq P_{\text{LOS}}(d_{aw})$, $P_{aw}(\text{N}) \triangleq 1 - P_{\text{LOS}}(d_{aw})$, $\Gamma(\cdot)$ is the gamma function [34, Eq. (8.310.1)], and $g_k^{(a,s)}$ and $b_k^{(a,s)}$ are defined above for $k \in \{1, 2\}$. Moreover, the*

function $S(\nu_{\mathcal{B}}, g_k^{(a,s)})$ is defined as

$$S(\nu_{\mathcal{B}}, g_k^{(a,s)}) \triangleq \sum_{l=1}^{\nu_{\mathcal{B}}} \binom{\nu_{\mathcal{B}}}{l} (-1)^l \left(1 + l \frac{\eta_{\mathcal{B}} P_J^{\max} g_k^{(a,s)}}{P_a m_{a,f} \nu_{\mathcal{B}}} \right)^{-\nu_{\mathcal{B}}}, \quad (14)$$

and $I(\nu_{\mathcal{B}}, l, g_k^{(a,s)})$, for $\nu_{\mathcal{B}} = 1$ and $\nu_{\mathcal{B}} \geq 2$, is defined as

$$I(1, l, g_k^{(a,s)}) \triangleq \ln \left(1 + l \frac{P_J^{\max} g_k^{(a,s)}}{P_a m_{a,f}} \right), \quad (15)$$

$$I(\nu_{\mathcal{B}} \geq 2, l, g_k^{(a,s)}) \triangleq \frac{(\nu_{\mathcal{B}} - 2)!}{\nu_{\mathcal{B}}^{\nu_{\mathcal{B}} - 1}} \left[1 - \left(1 + l \frac{\eta_{\mathcal{B}} P_J^{\max} g_k^{(a,s)}}{P_a m_{a,f} \nu_{\mathcal{B}}} \right)^{-\nu_{\mathcal{B}} + 1} \right]. \quad (16)$$

Proof: Let $P_{e,w}^C$, λ_1^C , and λ_2^C denote the values of $P_{e,w}^*$, λ_1 , and λ_2 , respectively, conditioned on the blockage instance $\mathcal{B} \in \{\text{L}, \text{N}\}$ and the gain $g^{(a,s)}$ of Alice's second array to Willie. Then using (9) we have

$$\begin{aligned} \mathbb{E}[P_{e,w}^C] &= \mathbb{E}_{\lambda_1^C < \lambda_2^C} [P_{e,w}^C] \Pr(\lambda_1^C < \lambda_2^C) + \mathbb{E}_{\lambda_1^C \geq \lambda_2^C} [P_{e,w}^C] \Pr(\lambda_1^C \geq \lambda_2^C) \\ &= \Pr(\lambda_1^C \geq \lambda_2^C) \left(1 - \frac{P_a m_{a,f}}{P_J^{\max} g^{(a,s)}} \mathbb{E}_{\lambda_1^C \geq \lambda_2^C} \left[\frac{|\tilde{h}_{aw,f}^{(\mathcal{B})}|^2}{|\tilde{h}_{aw,s}^{(\mathcal{B})}|^2} \right] \right). \end{aligned} \quad (17)$$

The closed form of $\Pr(\lambda_1^C \geq \lambda_2^C)$ is derived as

$$\begin{aligned} \Pr(\lambda_1^C \geq \lambda_2^C) &= \Pr \left(|\tilde{h}_{aw,f}^{(\mathcal{B})}|^2 \leq \frac{P_J^{\max} g^{(a,s)}}{P_a m_{a,f}} |\tilde{h}_{aw,s}^{(\mathcal{B})}|^2 \right) \\ &\stackrel{(a)}{=} \sum_{l=0}^{\nu_{\mathcal{B}}} \binom{\nu_{\mathcal{B}}}{l} (-1)^l \mathbb{E}_{|\tilde{h}_{aw,s}^{(\mathcal{B})}|^2} \left[\exp \left(-\eta_{\mathcal{B}} l \frac{P_J^{\max} g^{(a,s)}}{P_a m_{a,f}} |\tilde{h}_{aw,s}^{(\mathcal{B})}|^2 \right) \right] \\ &\stackrel{(b)}{=} \sum_{l=0}^{\nu_{\mathcal{B}}} \binom{\nu_{\mathcal{B}}}{l} (-1)^l \left(1 + l \frac{\eta_{\mathcal{B}} P_J^{\max} g^{(a,s)}}{P_a m_{a,f} \nu_{\mathcal{B}}} \right)^{-\nu_{\mathcal{B}}}, \end{aligned} \quad (18)$$

where step (a) follows from Alzer's lemma [35], [27, Lemma 6] for a normalized gamma RV $X \sim \text{Gamma}(\nu_{\mathcal{B}}, 1/\nu_{\mathcal{B}})$, which states that $\Pr(X < x)$ is tightly approximated by $[1 - \exp(-\eta_{\mathcal{B}} x)]^{\nu_{\mathcal{B}}}$ where $\eta_{\mathcal{B}} = \nu_{\mathcal{B}} (\nu_{\mathcal{B}}!)^{-1/\nu_{\mathcal{B}}}$, and then applying the binomial theorem assuming $\nu_{\mathcal{B}}$ is an integer [27], i.e.,

$$F_X(x) = \sum_{l=0}^{\nu_{\mathcal{B}}} \binom{\nu_{\mathcal{B}}}{l} (-1)^l e^{-l \eta_{\mathcal{B}} x}. \quad (19)$$

Moreover, step (b) is derived using the moment generating function (MGF) of a normalized gamma RV X , i.e., $\mathbb{E}[e^{tX}] = (1 - t/\nu_{\mathcal{B}})^{-\nu_{\mathcal{B}}}$ for any $t < \nu_{\mathcal{B}}$.

$$\mathbb{E}[P_{e,w}^*] = \sum_{\mathcal{B} \in \{\text{L}, \text{N}\}} P_{aw}(\mathcal{B}) \sum_{k=1}^2 b_k^{(a,s)} \left[1 + S(\nu_{\mathcal{B}}, g_k^{(a,s)}) \right] \times \left[1 - S(\nu_{\mathcal{B}}, g_k^{(a,s)}) + \frac{P_a m_{a,f} \nu_{\mathcal{B}}^{\nu_{\mathcal{B}}}}{P_J^{\max} g_k^{(a,s)} \eta_{\mathcal{B}} \Gamma(\nu_{\mathcal{B}})} \sum_{l=1}^{\nu_{\mathcal{B}}} \binom{\nu_{\mathcal{B}}}{l} \frac{(-1)^l}{l} I(\nu_{\mathcal{B}}, l, g_k^{(a,s)}) \right]. \quad (13)$$

Moreover, for the expectation term in (17) we have

$$\begin{aligned} & \mathbb{E}_{\lambda_1^C \geq \lambda_2^C} \left[\frac{|\tilde{h}_{aw,f}^{(B)}|^2}{|\tilde{h}_{aw,s}^{(B)}|^2} \right] \\ &= \mathbb{E} \left[\frac{|\tilde{h}_{aw,f}^{(B)}|^2}{|\tilde{h}_{aw,s}^{(B)}|^2} \left| \tilde{h}_{aw,f}^{(B)}|^2 \leq \frac{P_J^{\max} g^{(a,s)}}{P_a m_{a,f}} |\tilde{h}_{aw,s}^{(B)}|^2 \right. \right] \\ &= \int_0^\infty \frac{f_{|\tilde{h}_{aw,s}^{(B)}|^2}(y)}{y} \left[\underbrace{\int_0^{C_1 y} x f_{|\tilde{h}_{aw,f}^{(B)}|^2}(x) dx}_{V_1} \right] dy, \quad (20) \end{aligned}$$

where $C_1 \triangleq \frac{P_J^{\max} g^{(a,s)}}{P_a m_{a,f}}$, and $f_{|\tilde{h}_{aw,f}^{(B)}|^2}(x)$ and $f_{|\tilde{h}_{aw,s}^{(B)}|^2}(y)$ are the PDFs of the fading coefficients $|\tilde{h}_{aw,f}^{(B)}|^2$ and $|\tilde{h}_{aw,s}^{(B)}|^2$, respectively. Applying the part-by-part integration rule to V_1 and then using Alzer's lemma together with the binomial theorem as (19) yields

$$\begin{aligned} V_1 &= C_1 y \sum_{l_1=0}^{\nu_B} \binom{\nu_B}{l_1} (-1)^{l_1} e^{-l_1 \eta_B C_1 y} \\ &\quad - C_1 y - \sum_{l_2=1}^{\nu_B} \binom{\nu_B}{l_2} \frac{(-1)^{l_2}}{\eta_B l_2} [1 - e^{-l_2 \eta_B C_1 y}]. \quad (21) \end{aligned}$$

By plugging (21) into (20), using the MGF of the normalized gamma RV $|\tilde{h}_{aw,s}^{(B)}|^2$, and then noting that $f_{|\tilde{h}_{aw,s}^{(B)}|^2}(y) = \nu_B^{\nu_B} y^{\nu_B-1} e^{-\nu_B y} / \Gamma(\nu_B)$ we have

$$\begin{aligned} & \mathbb{E}_{\lambda_1^C \geq \lambda_2^C} \left[\frac{|\tilde{h}_{aw,f}^{(B)}|^2}{|\tilde{h}_{aw,s}^{(B)}|^2} \right] = C_1 \sum_{l_1=1}^{\nu_B} \binom{\nu_B}{l_1} (-1)^{l_1} \left(1 + l_1 \frac{\eta_B C_1}{\nu_B} \right)^{-\nu_B} \\ &\quad - \sum_{l_2=1}^{\nu_B} \binom{\nu_B}{l_2} \frac{(-1)^{l_2} \nu_B^{\nu_B}}{\eta_B l_2 \Gamma(\nu_B)} \left[\int_0^\infty y^{\nu_B-2} e^{-\nu_B y} dy \right. \\ &\quad \quad \left. - \int_0^\infty y^{\nu_B-2} e^{-(l_2 \eta_B C_1 + \nu_B) y} dy \right]. \quad (22) \end{aligned}$$

Now given that the parameter ν_B of Nakagami- m fading is always greater than or equal to 0.5 and is assumed to be an integer here, we have $\nu_B \in \mathbb{N}$ where \mathbb{N} stands for the set of natural numbers. For $\nu_B \geq 2$, by [34, Eq. (3.351.3)] we have $\int_0^\infty y^{\nu_B-2} e^{-\alpha y} dy = (\nu_B - 2)! / \alpha^{\nu_B-1}$ for any $\alpha \in \mathbb{R}^+$. On the other hand, for $\nu_B = 1$ using [34, Eq. (2.325.1)] we have $\int_0^\infty y^{-1} e^{-\alpha y} dy = \text{Ei}(-\alpha y)|_0^\infty$, where $\text{Ei}(\cdot)$ is the exponential integral function defined as [34, Eq. (8.211.1)] for negative arguments. Therefore, following a similar approach to the proof of [36, Corollary 2] we can calculate the difference of the two integrals in (22) as $\lim_{y \rightarrow 0} [\text{Ei}(-(l_2 \eta_B C_1 + \nu_B) y) - \text{Ei}(-\nu_B y)] = \ln([l_2 \eta_B C_1 + \nu_B] / \nu_B)$ which is equal to $\ln(1 + l_2 C_1)$ for $\nu_B = 1$ (note that $\eta_B = 1$ for $\nu_B = 1$, and $\text{Ei}(-\infty) = 0$). This completes the proof of the theorem given the definition of $I(\nu_B, l, g^{(a,s)})$ in Theorem 2. ■

Remark 2. In Theorem 2, it is assumed that Willie is not in the main lobe of Alice's first antenna array and hence, receives the desired signal by a side lobe gain $m_{a,f}$. However, if Willie is within the main lobe of the first array, we should include another averaging over the gain $g^{(a,f)}$ of the first array given the beamsteering error, i.e., that gain is either $g_1^{(a,f)} \triangleq M_{a,f}$ with probability $b_1^{(a,f)} \triangleq F_{|\mathcal{E}_{a,f}|}(\theta_{a,f}/2)$ or $g_2^{(a,f)} \triangleq m_{a,f}$ with probability $b_2^{(a,f)} \triangleq 1 - F_{|\mathcal{E}_{a,f}|}(\theta_{a,f}/2)$.

IV. PERFORMANCE OF THE ALICE-BOB LINK

In this section, we characterize performance metrics of the Alice-Bob link including its outage probability, maximum effective covert rate (i.e., the rate for which Alice can reliably communicate with Bob while maintaining $\mathbb{E}[P_{e,w}^*] \geq 1 - \epsilon$ for any $\epsilon > 0$), and ergodic capacity.

A. Outage Probability

We assume that Alice targets a rate R_b requiring the Alice-Bob link to meet a threshold signal-to-interference-plus-noise ratio (SINR) $\gamma_{\text{th}} \triangleq 2^{R_b} - 1$. Then the outage probability $P_{\text{out}}^{\text{AB}} \triangleq \Pr(\gamma_{ab} < \gamma_{\text{th}})$ in achieving R_b is characterized in Theorem 3, where the SINR γ_{ab} of the Alice-Bob link is given as follows by using (2):

$$\gamma_{ab} = \frac{P_a G_{ab,f} L_{ab} |\tilde{h}_{ab,f}|^2}{P_J G_{ab,s} L_{ab} |\tilde{h}_{ab,s}|^2 + \sigma_b^2}. \quad (23)$$

Note that in addition to $|\tilde{h}_{ab,f}|^2$, $|\tilde{h}_{ab,s}|^2$, and P_J , the blockage instance $\mathcal{B} \in \{\text{L}, \text{N}\}$ and the antenna gains can also change randomly across transmission blocks. In particular, while we assume that the jamming signal arrives with the deterministic side lobe gain $m_{a,s}$, there are still uncertainties in the gains of Alice's first array and Bob's receiver (they are pointing their main lobes) due to the beamsteering error. Therefore, the gain $g^{(a,f)}$ of the main lobe of Alice's first array pointed to Bob is either $g_1^{(a,f)} \triangleq M_{a,f}$ with probability $b_1^{(a,f)} \triangleq F_{|\mathcal{E}_{a,f}|}(\theta_{a,f}/2)$ or $g_2^{(a,f)} \triangleq m_{a,f}$ with probability $b_2^{(a,f)} \triangleq 1 - F_{|\mathcal{E}_{a,f}|}(\theta_{a,f}/2)$. Similarly, the gain $g^{(b)}$ of Bob's receiver is either $g_1^{(b)} \triangleq M_b$ with probability $b_1^{(b)} \triangleq F_{|\mathcal{E}_b|}(\theta_b/2)$ or $g_2^{(b)} \triangleq m_b$ with probability $b_2^{(b)} \triangleq 1 - F_{|\mathcal{E}_b|}(\theta_b/2)$. Furthermore, in Theorem 3 we assume that Willie is not in the main lobe of Alice's first array. However, if Willie is in the Alice-Bob direction, we should include another averaging of the gain of Alice's second array carrying the jammer signal, i.e., instead of a deterministic $m_{a,s}$ we should consider two possibilities $g_k^{(a,s)}$ with probabilities $b_k^{(a,s)}$, $k \in \{1, 2\}$, defined in Section III-B.

Theorem 3. The outage probability of the Alice-Bob link in achieving the target rate $R_b \triangleq \log_2(1 + \gamma_{\text{th}})$ is given by

$$\begin{aligned} P_{\text{out}}^{\text{AB}} &= \sum_{\mathcal{B} \in \{\text{L}, \text{N}\}} P_{ab}(\mathcal{B}) \sum_{k_1=1}^2 b_{k_1}^{(a,f)} \sum_{k_2=1}^2 b_{k_2}^{(b)} \left[1 + \sum_{l=1}^{\nu_B} \binom{\nu_B}{l} (-1)^l \right. \\ &\quad \left. \times \exp\left(-\frac{l \eta_B \gamma_{\text{th}} \sigma_b^2}{P_a g_{k_1}^{(a,f)} g_{k_2}^{(b)} L_{ab}}\right) V(\nu_B, l, g_{k_1}^{(a,f)}) \right], \quad (24) \end{aligned}$$

where $P_{ab}(\text{L}) \triangleq P_{\text{LOS}}(d_{ab})$ and $P_{ab}(\text{N}) \triangleq 1 - P_{\text{LOS}}(d_{ab})$. Also, $V(\nu_B, l, g_{k_1}^{(a,f)})$, for $\nu_B = 1$ and $\nu_B \geq 2$, is defined as

$$\begin{aligned} V(1, l, g_{k_1}^{(a,f)}) &\triangleq \frac{P_a g_{k_1}^{(a,f)}}{P_J^{\max} l \gamma_{\text{th}} m_{a,s}} \ln\left(1 + \frac{P_J^{\max} l \gamma_{\text{th}} m_{a,s}}{P_a g_{k_1}^{(a,f)}}\right), \quad (25) \\ V(\nu_B \geq 2, l, g_{k_1}^{(a,f)}) &\triangleq \frac{\nu_B P_a g_{k_1}^{(a,f)}}{P_J^{\max} l \eta_B \gamma_{\text{th}} m_{a,s} (\nu_B - 1)} \\ &\quad \times \left[1 - \left(1 + \frac{P_J^{\max} l \eta_B \gamma_{\text{th}} m_{a,s}}{\nu_B P_a g_{k_1}^{(a,f)}}\right)^{1-\nu_B} \right]. \quad (26) \end{aligned}$$

Proof: Given the SINR of the Alice-Bob link in (23), the outage probability conditioned on the blockage instance \mathcal{B} as well as the antenna gains $g^{(a,f)}$ and $g^{(b)}$ is characterized as follows:

$$\begin{aligned}
P_{\text{out},C}^{\text{AB}} &\triangleq \Pr(\gamma_{ab} < \gamma_{\text{th}} | \mathcal{B}, g^{(a,f)}, g^{(b)}) \\
&\stackrel{(a)}{=} \Pr\left(|\tilde{h}_{ab,f}^{(\mathcal{B})}|^2 < C_2 P_J |\tilde{h}_{ab,s}^{(\mathcal{B})}|^2 + C_3\right) \\
&\stackrel{(b)}{=} \sum_{l=0}^{\nu_{\mathcal{B}}} \binom{\nu_{\mathcal{B}}}{l} (-1)^l e^{-l\eta_{\mathcal{B}} C_3} \mathbb{E}_{P_J, |\tilde{h}_{ab,s}^{(\mathcal{B})}|^2} \left[e^{-l\eta_{\mathcal{B}} C_2 P_J |\tilde{h}_{ab,s}^{(\mathcal{B})}|^2} \right] \\
&\stackrel{(c)}{=} \sum_{l=0}^{\nu_{\mathcal{B}}} \binom{\nu_{\mathcal{B}}}{l} (-1)^l e^{-l\eta_{\mathcal{B}} C_3} \mathbb{E}_{P_J} \left[\left(1 + \frac{l\eta_{\mathcal{B}} C_2 P_J}{\nu_{\mathcal{B}}} \right)^{-\nu_{\mathcal{B}}} \right] \\
&\stackrel{(d)}{=} 1 + \sum_{l=1}^{\nu_{\mathcal{B}}} \binom{\nu_{\mathcal{B}}}{l} \frac{(-1)^l e^{-l\eta_{\mathcal{B}} C_3}}{P_J^{\max}} \int_0^{P_J^{\max}} \left(1 + \frac{l\eta_{\mathcal{B}} C_2 x}{\nu_{\mathcal{B}}} \right)^{-\nu_{\mathcal{B}}} dx, \quad (27)
\end{aligned}$$

where in step (a) we have defined $C_2 \triangleq \gamma_{\text{th}} m_{a,s} / (P_a g^{(a,f)})$ and $C_3 \triangleq \gamma_{\text{th}} \sigma_b^2 / (P_a g^{(a,f)} g^{(b)} L_{ab}^{(\mathcal{B})})$. Moreover, step (b) follows by Alzer's lemma together with the binomial theorem as (19), and step (c) is derived using the MGF of the normalized gamma RV $|\tilde{h}_{ab,s}^{(\mathcal{B})}|^2$. Finally, taking the integral in step (d) and recalling the definition of the function $V(\nu_{\mathcal{B}}, l, g_{k_1}^{(a,f)})$ from the statement of the theorem complete the proof. ■

B. Maximum Effective Covert Rate

Given any target data rate R_b , Alice and Bob can have the effective communication rate $\bar{R}_{a,b} \triangleq R_b(1 - P_{\text{out}}^{\text{AB}})$, where their outage probability $P_{\text{out}}^{\text{AB}}$ in achieving the target rate R_b is obtained using Theorem 3. The goal here is to determine the optimal value of P_J^{\max} that maximizes $\bar{R}_{a,b}$ while also satisfying the covertness requirement, i.e., $\mathbb{E}[P_{e,w}^*] \geq 1 - \epsilon$ for any $\epsilon > 0$. We first note that $\mathbb{E}[P_{e,w}^*]$ and $P_{\text{out}}^{\text{AB}}$ both monotonically increase with P_J^{\max} (see also Fig. 1 and Fig. 2 for the visualization). Then, in order to obtain the maximum effective covert rate $\bar{R}_{a,b}^*$ achievable in our setup, we need to pick the smallest possible value for P_J^{\max} given that $\bar{R}_{a,b}$ is monotonically decreasing with respect to P_J^{\max} . This smallest possible value for P_J^{\max} , denoted by $P_{J,\text{opt}}^{\max}$, must also satisfy the covertness requirement $\mathbb{E}[P_{e,w}^*] \geq 1 - \epsilon$ for any $\epsilon > 0$. Now, given that $\mathbb{E}[P_{e,w}^*]$ monotonically increases with P_J^{\max} , the solution of the equation $\mathbb{E}[P_{e,w}^*] = 1 - \epsilon$ for P_J^{\max} defines $P_{J,\text{opt}}^{\max}$. This observation is summarized in the following proposition. Note, however, that the optimal rate per Proposition 4 needs to be evaluated numerically.

Proposition 4. *Given fixed system and channel parameters, fixed covertness requirement ϵ , and target data rate R_b , the maximum effective covert rate achievable in the considered setup is equal to $R_b(1 - P_{\text{out}}^{\text{AB}})$, denoted by $\bar{R}_{a,b}^*$, where $P_{\text{out}}^{\text{AB}}$ is equal to $P_{\text{out}}^{\text{AB}}$, specified in (24), evaluated in $P_{J,\text{opt}}^{\max}$ that is the solution of the equation $\mathbb{E}[P_{e,w}^*] = 1 - \epsilon$ for P_J^{\max} .*

C. Ergodic Capacity

In addition to characterizing the maximum effective covert rate $\bar{R}_{a,b}^*$ given a target rate R_b , provided in Section IV-B, it is desirable to determine the achievable average data rate of the

Alice-Bob link, referred to as its *ergodic capacity*, given fixed values for the parameters involved in the model¹. The ergodic capacity $\mathbb{E}[R_{a,b}]$ of the Alice-Bob link is obtained while assuming that the threshold/target data rate R_b is adjusted by the channel conditions, i.e., $\gamma_{\text{th}} = \gamma_{ab}$, implying that Bob's decoder can always decode the received signal without outage. In fact, given the instantaneous SINR γ_{ab} , specified in (23), Alice can reliably transmit to Bob with the data rate equal to $\log_2(1 + \gamma_{ab})$. Therefore, on average, the data rate $\mathbb{E}[R_{a,b}] \triangleq \mathbb{E}[\log_2(1 + \gamma_{ab})]$ is achievable for the Alice-Bob link, where the expectation is over the RVs involved in (23). In the following theorem, we characterize $\mathbb{E}[R_{a,b}]$ in a tractable form that involves only one-dimensional integrals over one of the fading coefficients.

Theorem 5. *The ergodic capacity $\mathbb{E}[R_{a,b}]$ of the Alice-Bob link is given by*

$$\begin{aligned}
\mathbb{E}[R_{a,b}] &= \frac{P_a}{m_{a,s} P_J^{\max} \ln 2} \sum_{\mathcal{B} \in \{\mathcal{L}, \mathcal{N}\}} P_{ab}(\mathcal{B}) \sum_{k_1=1}^2 b_{k_1}^{(a,f)} g_{k_1}^{(a,f)} \\
&\quad \times \sum_{k_2=1}^2 b_{k_2}^{(b)} \sum_{l=1}^{\nu_{\mathcal{B}}} \binom{\nu_{\mathcal{B}}}{l} \frac{(-1)^l}{l\eta_{\mathcal{B}}} [\mathcal{J}_1 - \mathcal{J}_2 - \mathcal{J}_3], \quad (28)
\end{aligned}$$

where \mathcal{J}_1 , \mathcal{J}_2 , and \mathcal{J}_3 are defined in the form of one-dimensional integrals as follows:

$$\mathcal{J}_1 \triangleq \int_0^\infty \frac{1}{y} \left[\text{eEi} \left(\frac{l\eta_{\mathcal{B}}}{P_a g_{k_1}^{(a,f)}} \left[m_{a,s} P_J^{\max} y + \frac{\sigma_b^2}{g_{k_2}^{(b)} L_{ab}^{(\mathcal{B})}} \right] \right) \right] f_Y(y) dy, \quad (29)$$

$$\mathcal{J}_2 \triangleq \left[\text{eEi} \left(\frac{l\eta_{\mathcal{B}} \sigma_b^2}{P_a g_{k_1}^{(a,f)} g_{k_2}^{(b)} L_{ab}^{(\mathcal{B})}} \right) \right] \int_0^\infty \frac{1}{y} f_Y(y) dy, \quad (30)$$

$$\mathcal{J}_3 \triangleq \int_0^\infty \frac{1}{y} \left[\ln \left(1 + \frac{m_{a,s} g_{k_2}^{(b)} L_{ab}^{(\mathcal{B})} P_J^{\max}}{\sigma_b^2} y \right) \right] f_Y(y) dy, \quad (31)$$

where $\text{eEi}(x) \triangleq e^x \text{Ei}(-x)$, and $f_Y(y)$ is the PDF of a normalized gamma RV as in (1).

Proof: Based on the system model considered in this paper and our earlier discussions, we have

$$\mathbb{E}[R_{a,b}] = \sum_{\mathcal{B} \in \{\mathcal{L}, \mathcal{N}\}} P_{ab}(\mathcal{B}) \sum_{k_1=1}^2 b_{k_1}^{(a,f)} \sum_{k_2=1}^2 b_{k_2}^{(b)} \mathbb{E}[R_{a,b} | \mathcal{B}, g^{(a,f)}, g^{(b)}], \quad (32)$$

where $\mathbb{E}[R_{a,b} | \mathcal{B}, g^{(a,f)}, g^{(b)}]$ is the ergodic capacity conditioned on the blockage instance \mathcal{B} , and the antenna gains $g^{(a,f)}$ and $g^{(b)}$. Given the definition of the ergodic capacity $\mathbb{E}[R_{a,b}] \triangleq \mathbb{E}[\log_2(1 + \gamma_{ab})]$ and the expression of the SINR

¹We assume that the set of parameters is chosen such that the covert communication requirement $\mathbb{E}[P_{e,w}^*] \geq 1 - \epsilon$ is satisfied for any $\epsilon > 0$. Note that $\mathbb{E}[P_{e,w}^*]$ depends only on the values of the design parameters as well as the statistics of the RVs involved and not on their instantaneous realizations.

γ_{ab} in (23), we have

$$\mathbb{E}[R_{a,b}|\mathcal{B}, g^{(a,f)}, g^{(b)}] = \mathbb{E}_{Y,P_J} \left[\int_0^\infty \log_2(1 + C'_1 x) f_X(x) dx \right], \quad (33)$$

where $X \triangleq |\tilde{h}_{ab,f}^{(\mathcal{B})}|$ and $Y \triangleq |\tilde{h}_{ab,s}^{(\mathcal{B})}|$ represent the RVs associated with the involved fading coefficients with PDFs $f_X(x)$ and $f_Y(y)$, respectively. Moreover, $C'_1 \triangleq 1/(C'_2 P_J Y + C'_3)$ with $C'_2 \triangleq m_{a,s}/(P_a g^{(a,f)})$ and $C'_3 \triangleq \sigma_b^2/(P_a g^{(a,f)} g^{(b)} L_{ab}^{(\mathcal{B})})$. Observe that for a given RV Z with the PDF $f_Z(z)$ and CDF $F_Z(z)$ we have the following part-by-part integration equality

$$\int_a^b \log_2(1 + cz) f_Z(z) dz = \frac{1}{\ln 2} \left[c \int_a^b \frac{1 - F_Z(z)}{1 + cz} dz + (1 - F_Z(a)) \ln(1 + ca) - (1 - F_Z(b)) \ln(1 + cb) \right], \quad (34)$$

with c being a constant. Then the integral involved in (33) is computed as follows:

$$\begin{aligned} \int_0^\infty \log_2(1 + C'_1 x) f_X(x) dx &\stackrel{(a)}{=} \frac{C'_1}{\ln 2} \int_0^\infty \frac{1 - F_X(x)}{1 + C'_1 x} dx \\ &\stackrel{(b)}{=} \frac{1}{\ln 2} \sum_{l=1}^{\nu_{\mathcal{B}}} \binom{\nu_{\mathcal{B}}}{l} (-1)^l e^{l\eta_{\mathcal{B}}/C'_1} \text{Ei}(-l\eta_{\mathcal{B}}/C'_1), \end{aligned} \quad (35)$$

where step (a) is by using (34), and noting that $(1 - F_X(0)) \ln(1 + C'_1 \times 0) = 0$ and

$$\lim_{x \rightarrow \infty} (1 - F_X(x)) \ln(1 + C'_1 x) = 0, \quad (36)$$

since $1 - F_X(x) = -\sum_{l=1}^{\nu_{\mathcal{B}}} \binom{\nu_{\mathcal{B}}}{l} (-1)^l e^{-l\eta_{\mathcal{B}} x}$ decays exponentially while $\ln(1 + C'_1 x)$ grows logarithmically with x . Moreover, step (b) is derived by first using Alzer's lemma together with the binomial theorem as (19), and then applying [34, Eq. (3.352.4)]. Now by substituting (35) into (33), we have for the conditional ergodic capacity

$$\mathbb{E}[R_{a,b}|\mathcal{B}, g^{(a,f)}, g^{(b)}] = \frac{1}{P_J^{\max} \ln 2} \sum_{l=1}^{\nu_{\mathcal{B}}} \binom{\nu_{\mathcal{B}}}{l} (-1)^l \mathbb{E}_Y \left[\underbrace{\int_0^{P_J^{\max}} \exp(l\eta_{\mathcal{B}}(C'_2 Y t + C'_3)) \text{Ei}(-l\eta_{\mathcal{B}}(C'_2 Y t + C'_3)) dt}_{I_1} \right]. \quad (37)$$

The integral term I_1 can be computed in a closed form as

$$\begin{aligned} I_1 &\stackrel{(a)}{=} \frac{1}{C'_2 Y} \int_{C'_3}^{C'_2 Y P_J^{\max} + C'_3} \exp(l\eta_{\mathcal{B}} z) \text{Ei}(-l\eta_{\mathcal{B}} z) dz \\ &\stackrel{(b)}{=} \frac{1}{l\eta_{\mathcal{B}} C'_2 Y} \left[\text{eEi}(l\eta_{\mathcal{B}}(C'_2 Y P_J^{\max} + C'_3)) - \text{eEi}(l\eta_{\mathcal{B}} C'_3) - \ln(1 + C'_2 Y P_J^{\max}/C'_3) \right], \end{aligned} \quad (38)$$

where step (a) is by defining $z \triangleq C'_2 Y t + C'_3$, and step (b) is obtained using Lemma 7 in Appendix A and defining $\text{eEi}(x) \triangleq e^x \text{Ei}(-x)$. Finally, taking the expectation of I_1 in (38) over Y and then plugging (37) back into (32) complete the proof. ■

To the best of our knowledge, the one-dimensional integrals in (29)-(31) cannot be computed in closed forms for all values of $\nu_{\mathcal{B}}$. In particular, obtaining closed-form expressions for the special case $\nu_{\mathcal{B}} = 1$, which corresponds to Rayleigh fading channels, is not straightforward mainly due to the fractional term $1/y$ in the integrands. On the other hand, as delineated in the following proposition, deriving the closed forms of (29)-(31) for the special case $\nu_{\mathcal{B}} = 2$ is straightforward.

Proposition 6. For $\nu_{\mathcal{B}} = 2$, the closed-form expressions for \mathcal{J}_1 , \mathcal{J}_2 , and \mathcal{J}_3 , defined in Theorem 5, are as follows:

$$\mathcal{J}_1 = \frac{4P_a g_{k_1}^{(a,f)}}{l\eta_{\mathcal{B}} m_{a,s} P_J^{\max} - 2P_a g_{k_1}^{(a,f)}} \left[\text{eEi} \left(\frac{2\sigma_b^2}{g_{k_2}^{(b)} L_{ab}^{(\mathcal{B})} m_{a,s} P_J^{\max}} \right) - \text{eEi} \left(\frac{l\eta_{\mathcal{B}} \sigma_b^2}{P_a g_{k_1}^{(a,f)} g_{k_2}^{(b)} L_{ab}^{(\mathcal{B})}} \right) \right], \quad (39)$$

$$\mathcal{J}_2 = 2 \text{eEi} \left(\frac{l\eta_{\mathcal{B}} \sigma_b^2}{P_a g_{k_1}^{(a,f)} g_{k_2}^{(b)} L_{ab}^{(\mathcal{B})}} \right), \quad (40)$$

$$\mathcal{J}_3 = -2 \text{eEi} \left(\frac{2\sigma_b^2}{m_{a,s} g_{k_2}^{(b)} L_{ab}^{(\mathcal{B})} P_J^{\max}} \right). \quad (41)$$

Proof: The proof follows by replacing $f_Y(y) = 4ye^{-2y}$. Then the closed forms for \mathcal{J}_1 and \mathcal{J}_3 are derived by applying [36, Corollary 1] and [34, Eq. (4.337.2)], respectively. ■

It is worth mentioning at the end that rather complicated closed forms can also be obtained for the case of $\nu_{\mathcal{B}} > 2$ by employing, e.g., [37, Eq. (06.35.21.0016.01)], [34, Eq. (3.351.3)], and [34, Eq. (4.358.1)] to solve the integrals involved in (29), (30), and (31), respectively.

V. PRACTICAL SCENARIOS, DISCUSSIONS, AND FUTURE DIRECTIONS

In this section, we first describe the localization issue in covert mmWave communications and propose a potential design approach that can be incorporated in the context of the system model in this paper. We then establish how the performance metrics of the proposed scheme can be characterized using the earlier results in this paper. Finally, we highlight several interesting future research directions.

A. Localization Issue

One of the important aspects in the design of a typical mmWave communication network is the localization of the nodes. This is mainly due to the vulnerability of mmWave links, comprised of directive beams, to the blockage. In the context of the system model in this paper, while it is important in the design of the system to know both Bob's and Willie's locations, obtaining the information about Willie's location is ought to be much more challenging. In fact, the legitimate parties Alice and Bob can apply sophisticated beam training approaches to establish a directional link. However, since Willie is a passive node, it is more difficult for Alice to obtain precise information about Willie's location.

Speaking of Willie's location, both Alice's distance to Willie and the spatial direction between them are important to set

up the covert mmWave communication system. However, the distance between Alice and Willie is less challenging if the spatial direction between them is known or if the direction issue is properly addressed in the system design. In fact, all of our earlier derivations are in terms of the link length d_{aw} between Alice and Willie. Therefore, the performance metrics change with respect to the distance between Alice and Willie, and one needs to adopt a new set of values for the involved parameters to ensure the covertness requirement while, in the mean time, maximizing the effective rate between Alice and Bob. Note that the uncertainty about Alice's distance to Willie also exists in conventional RF-based covert communication systems incorporating omni-directional antennas and is not particular to the case of covert mmWave communication.

On the other hand, the uncertainty about the spatial direction between Alice and Willie is more challenging as it directly impacts the design architecture for Alice's transmitter. Throughout the paper we assumed that Willie's direction is known to Alice such that the main lobe of Alice's second antenna array, carrying the jamming signal, is pointed toward Willie. However, in the case of uncertainty about Willie's direction we might not be able to do that; as a result, the jamming signal may arrive to Willie with a much lower gain of the side lobe rather than the main lobe of the second array. This deteriorates the system performance by improving Willie's detection performance which in turn degrades the Alice-Bob link performance by, e.g., requiring Alice to employ lower signal powers P_a or larger jammer powers P_J^{\max} to satisfy the covertness requirement.

One immediate solution to address the aforementioned issue on the uncertainty about Willie's direction is to employ an antenna array with a wide (main lobe) beamwidth to transmit the jamming signal. However, it is very difficult to cover the whole space (except the Alice-Bob direction) using a single wide main lobe [38]. Therefore, Alice may prefer to employ several wide-beam antenna arrays to transmit the jamming signal. In this case, the main lobe of each array covers a certain spatial direction such that the union of the main lobes covers the whole space except the Alice-Bob direction. As a result, from the design perspective, we no longer need to know Willie's direction as the whole space is covered by multiple antenna arrays leaving a null space (or negligible side lobes) toward Bob's direction. However, from the analysis point of view, it is not easy to derive tractable forms for the system performance metrics as discussed next. In fact, assuming the sectored-pattern antenna model, as in Section II-A, each antenna array has a main lobe and a side lobe. Therefore, the jammer signal arrives at Willie by a main lobe from the antenna array covering the Alice-Willie direction in addition to several side lobes each from all other antenna arrays. Similarly, the jammer signal arrives at Bob by the side lobe of all arrays other than the first antenna array. Given the spatial distance between the antenna arrays, the channel between each side lobe and the receiver, either Willie or Bob, has to be assigned an independent fading coefficient. Therefore, the received signals by Willie and Bob involve several independent Nakagami fading coefficients making it difficult to derive tractable forms for the performance metrics.

In the next subsection, we elucidate how the results in the paper can be applied to approximate the performance metrics with respect to this multi-array system model that resolves the issue of uncertainty about Alice-Willie direction.

Remark 3. The system model considered in this paper and the subsequent analytical results are directly applicable to the case where an external jammer node with a single or multiple antenna arrays is used to transmit the jamming signal instead of (an) extra antenna array(s) in Alice.

B. Approximate Performance of the Multi-Array Transmitter

Consider a system model same as the one described in Section II-B except that Alice is equipped with N_J wide-beam arrays, instead of one, each carrying a same jamming signal and together covering the whole space except the Alice-Bob direction. The main lobe gain of the antenna arrays carrying the jamming signals is assumed to be the same, denoted by $M_{a,s}$. Now, we make the following two assumptions to approximate the system performance using tractable forms.

1- *Zero side lobe gains from jamming arrays to Willie:* Note that, regardless of Willie's location, the main portion of jamming signal reaches Willie by a main lobe gain $M_{a,s}$ from one of N_J arrays, denoted by the j_1 -th array, that is covering Willie's spatial direction. Then the received jamming signal by Willie at the i -th channel use is expressed as

$$\mathbf{y}_{w,J}(i) = \sqrt{P_J L_{aw} g^{(w)}} \mathbf{x}_J(i) \left[\tilde{h}_{aw,j_1} \sqrt{M_{a,s}} + \sum_{\substack{j'=1 \\ j' \neq j_1}}^{N_J} \tilde{h}_{aw,j'} \sqrt{m_{a,j'}} \right], \quad (42)$$

where $g^{(w)}$ is Willie's beamforming gain, $m_{a,j'}$ is the side lobe gain of the j' -th array, and $\tilde{h}_{aw,j'}$ is the fading coefficient from Alice's j' -th jamming array to Willie. Assuming that the main lobe gain is much larger than the side lobe gains, we can expect the summation term inside the bracket to have negligible contribution compared to the term $\tilde{h}_{aw,j_1} \sqrt{M_{a,s}}$ for *typical* realizations of channel fading coefficients. Note that the fading coefficients $\tilde{h}_{aw,j'}$'s have different phases and hence, the summation term does not blow up with N_J though N_J itself is relatively small given the wide beamwidths used. We can then approximate $\mathbf{y}_{w,J}(i)$ as

$$\mathbf{y}_{w,J}(i) \approx \sqrt{P_J L_{aw} M_{a,s} g^{(w)}} \tilde{h}_{aw,j_1} \mathbf{x}_J(i). \quad (43)$$

2- *A single side lobe from jamming arrays to Bob:* Same as in (42), the received jamming signal by Bob at the i -th channel use is expressed as

$$\begin{aligned} \mathbf{y}_{b,J}(i) &= \sqrt{P_J L_{ab} g^{(b)}} \mathbf{x}_J(i) \sum_{j''=1}^{N_J} \tilde{h}_{ab,j''} \sqrt{m_{a,j''}} \\ &\stackrel{(a)}{\approx} \sqrt{P_J L_{ab} m_{a,j_2} g^{(b)}} \tilde{h}_{ab,j_2} \mathbf{x}_J(i), \end{aligned} \quad (44)$$

where $\tilde{h}_{ab,j''}$ is the fading coefficient from Alice's j'' -th jamming array to Bob. Moreover, step (a) in (44) is obtained

by considering the largest side lobe gain, denoted by j_2 -th array, as the dominant term of the summation.

Now, given the above two assumptions, it is easy to observe that the performance of the new multi-array system model can be approximated according to our earlier results on the dual-array model. The only difference is that we no longer need to take the average over the gain of the jamming array to Willie to compute $\mathbb{E}[P_{e,w}^*]$ since that gain is deterministically equal to $M_{a,s}$ given the multi-array architecture. All the other derivations remain the same.

C. Future Directions

The research in this work can be extended in various directions. Moreover, given the distinct superiorities of covert communication over mmWave bands compared to that of RF systems, and that not much work is done in this area, significant effort is needed to fill the gap in the literature on various aspects of covert mmWave communication. In the following, we enumerate some interesting directions for future work.

1) *Uncertainty about Willie's location:* In Section V-A, we explained the importance of knowing Willie's location, i.e., his distance d_{aw} and spatial direction with respect to Alice. Although the system model and the subsequent analysis work well for all values of d_{aw} , it is desirable to explore how Alice's uncertainty about d_{aw} impacts the system performance, e.g., the effective covert rate (see, e.g., [21]). Furthermore, we proposed a multi-array design scheme that results in an omnidirectional transmission of the jamming signal and eliminates the need for precise information about the direction to Willie. Although omnidirectional transmission of the jamming signal (that can negatively impact all nearby nodes in the network rather than just Willie and Bob) is also the case in RF-based covert communication systems, one might be able to perform better in mmWave systems. Exploring potential approaches that enable obtaining partial information about Willie's location and then characterizing their performance, possibly under some uncertainty or imperfect knowledge, is a viable research direction.

2) *Precise performance characterization of the multi-array system model:* In Section V-B, we highlighted how the performance of the multi-array system model proposed in Section V-A can, *approximately*, be characterized using the analytical results in the paper. One might be able to provide a more rigorous analysis by eliminating the two assumptions made in Section V-B. To this end, some analytical tools, such as [39], to characterize the weighted sum of the involved RVs in (42) and (44) are potentially useful.

3) *Distribution of the jamming signal power P_J :* In the context of the system model in this paper, it is easy to verify that in the case of a constant (deterministic) P_J Willie can attain a zero detection error by choosing any threshold value in the interval $T_w^{\text{H}_0} < \tau < T_w^{\text{H}_1}$, where $T_w^{\text{H}_0}$ and $T_w^{\text{H}_1}$ are defined in (6) and (7), respectively. Therefore, achieving a positive-rate covert communication, as $n \rightarrow \infty$, is not possible since the covertness requirement $P_{e,w} \geq 1 - \epsilon$ cannot be met. In this paper, we considered a uniform distribution for P_J in the

TABLE II
PARAMETERS USED FOR THE NUMERICAL ANALYSIS.

Coefficients	Values
Link lengths (d_{aw}, d_{ab})	(25, 25) m
Path loss exponents (α_L, α_N)	(2, 4)
Path loss intercepts (C_L, C_N)	($10^{-7}, 10^{-7}$)
Main lobe gains ($M_{a,f}, M_{a,s}, M_b$)	(15, 15, 15) dB
Side lobe gains ($m_{a,f}, m_{a,s}, m_b$)	(-5, -5, -5) dB
Transmit power of Alice's first array, P_a	20 dBm
Noise power (σ_w^2, σ_b^2)	(-74, -74) dBm
Nakagami fading parameters (ν_L, ν_N)	(3, 2)
Array beamwidths ($\theta_{a,f}, \theta_{a,s}, \theta_b$)	($30^\circ, 30^\circ, 30^\circ$)
Beamsteering error parameter, Δ	5°

interval $[0, P_J^{\max}]$. Characterizing the performance metrics for the considered covert mmWave communication system model under other statistical distributions for P_J is a straightforward yet important follow-up research that can help determining the optimal/best distribution(s) for the jamming signal power.

4) *Covert mmWave communication under other potential system models:* In this paper, we have incorporated jamming signals with random realizations per transmission block to enable positive-rate covert mmWave communication in the limit of large blocklengths. One can explore covert mmWave communication under other potential system models, such as uncertainty about the channel gains, noise power, transmission blocks, etc, by utilizing results already established in the literature (see, e.g., [10]–[18]). In fact, based on the discussion in Section V-C3 and assuming no jammer in the system model ($P_J = 0$), Willie can attain a zero detection error by choosing any threshold value in the interval $\sigma_w^2 < \tau < P_a G_{aw,f} L_{aw} |\tilde{h}_{aw,f}|^2 + \sigma_w^2$. However, roughly speaking, Willie's uncertainty about the noise power and channel gains may prevent him from choosing threshold levels that guarantee a zero detection error for him. This motivates other potential system models that have to, of course, take into account the intrinsic properties of mmWave channels and systems.

5) *Fundamental information-theoretic studies:* While we mainly discussed *communication-theoretic* studies attempting to achieve positive-rate covert mmWave communication over large blocklengths, it is very important to fill the gap by *information-theoretic* studies trying to understand fundamental limits of covert mmWave communication, e.g., in the limit of short/medium blocklengths (see, e.g., [4]–[9]).

VI. NUMERICAL RESULTS

In this section, we provide numerical results for various performance metrics delineated in Theorem 2, Theorem 3, Proposition 4, and Theorem 5. The parameters listed in Table II are considered in our numerical analysis unless explicitly mentioned. It is assumed that the beamsteering error follows a Gaussian distribution with mean zero and variance Δ^2 ; hence, $F_{|\mathcal{E}|}(x) = \text{erf}(x/(\Delta\sqrt{2}))$ where $\text{erf}(\cdot)$ denotes the error function [26]. Moreover, the blockage model $P_{\text{LOS}}(d_{ij}) = e^{-d_{ij}/200}$ [22] is used throughout the numerical analysis.

Fig. 1 shows the expected value $\mathbb{E}[P_{e,w}^*]$ of Willie's detection error rate for a benchmark scenario, corresponding to the

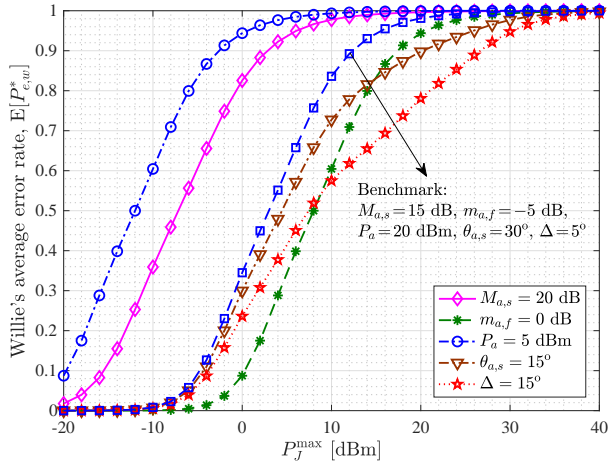


Fig. 1. The expected value $\mathbb{E}[P_{e,w}^*]$ of Willie's detection error rate for a benchmark scenario with $M_{a,s} = 15$ dB, $m_{a,f} = -5$ dB, $P_a = 20$ dBm, $\theta_{a,s} = 30^\circ$, and $\Delta = 5^\circ$. The effect of different parameters is explored by considering the values $M_{a,s} = 20$ dB, $m_{a,f} = 0$ dB, $P_a = 5$ dBm, $\theta_{a,s} = 15^\circ$, and $\Delta = 15^\circ$ while keeping the rest of the parameters exactly the same as the benchmark scenario.

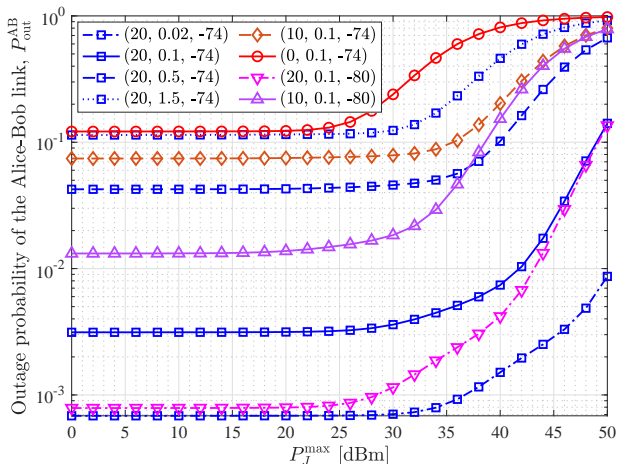


Fig. 2. The outage probability of the Alice-Bob link for various values of the transmit power P_a , threshold rate R_b , and noise variance σ_b^2 . The elements of the triples in the legend are P_a in dBm, R_b , and σ_b^2 in dBm, respectively.

parameters listed in Table II, as a function of P_J^{\max} . Moreover, the impact of some relevant parameters, i.e., $M_{a,s}$, $m_{a,f}$, P_a , $\theta_{a,s}$, and Δ is evaluated by changing each of these parameters while keeping the rest of the parameters exactly the same as the benchmark scenario. As expected, $\mathbb{E}[P_{e,w}^*]$ monotonically increases with P_J^{\max} . Also, reducing P_a degrades Willie's performance since the power level of the desired signal is reduced making it more difficult to be detectable by Willie. Moreover, increasing $M_{a,s}$ deteriorates Willie's performance by exposing his receiver to a more intense jamming signal. On the other hand, decreasing $\theta_{a,s}$ or increasing Δ decrease $\mathbb{E}[P_{e,w}^*]$ since they reduce the probability of Willie receiving the jamming signal with the main lobe of Alice's second array. Finally, increasing $m_{a,f}$ also improves Willie's performance by revealing a higher level of the desired signal, gained by $m_{a,f}$, to Willie.

The outage probability of the Alice-Bob link is illustrated in

TABLE III
COVERT RATES FOR $\epsilon = 0.05$ AND VARIOUS THRESHOLD RATES.

R_b	0.1	0.5	1	2.5	5	10
P_{out}^{*AB}	0.00314	0.04253	0.0935	0.121	0.1308	0.9913
$\bar{R}_{a,b}^*$	0.0997	0.4787	0.9065	2.1975	4.3459	0.0866

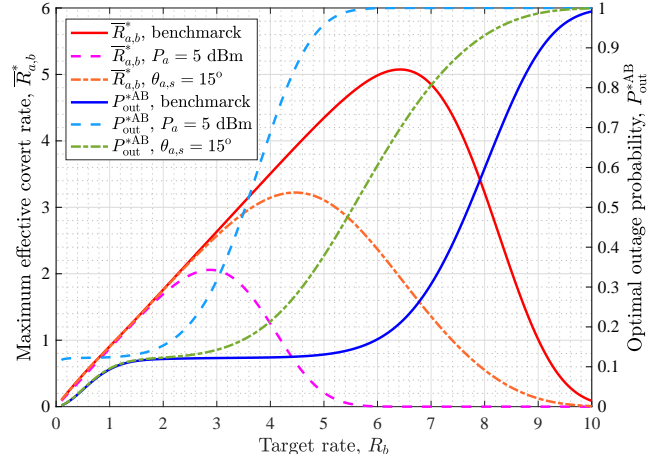


Fig. 3. The effective covert rate $\bar{R}_{a,b}^*$ and the corresponding optimal outage probability P_{out}^{*AB} as a function of target rate R_b . In addition to the benchmark scenario, two other scenarios of Fig. 1, namely those obtained by changing P_a from 20 dBm to 5 dBm, and $\theta_{a,s}$ from 30° to 15° , are also considered.

Fig. 2 for various values of the transmit power P_a , threshold rate R_b , and noise variance σ_b^2 . The rest of the parameters are the same as those in Table II. As expected, P_{out}^{*AB} monotonically increases with P_J^{\max} . Moreover, the reliability of Alice-to-Bob transmission degrades by increasing the threshold rate R_b and the noise variance σ_b^2 while increasing P_a improves the performance.

Effective covert rates corresponding to the benchmark scenario in Fig. 1 are summarized in Table III for $\epsilon = 0.05$ and various threshold rates. To obtain these results, we first numerically solved the equation $\mathbb{E}[P_{e,w}^*] = 1 - \epsilon$ for P_J^{\max} , given the parameters corresponding to the benchmark scenario. This resulted in the optimal value of $P_{J,\text{opt}}^{\max} = 15.52$ dBm. Then we computed the corresponding optimal outage probabilities P_{out}^{*AB} , for various target rates, according to Theorem 3. The effective covert rate $\bar{R}_{a,b}^*$ and the corresponding optimal outage probability P_{out}^{*AB} for the considered benchmark scenario is also plotted, as a function of target rate R_b , in Fig. 3. Furthermore, Fig. 3 includes the results of $\bar{R}_{a,b}^*$ and P_{out}^{*AB} for two other scenarios of Fig. 1, namely those obtained by changing P_a from 20 dBm to 5 dBm, and $\theta_{a,s}$ from 30° to 15° . It is observed that, for a given link, the effective covert rate first increases and then decreases by increasing the threshold rate. The maximum effective covert rate that is achievable for the benchmark scenario is 5.0743 that is obtained for the target rate of $R_b = 6.42$ with the corresponding optimal outage probability of $P_{\text{out}}^{*AB} = 0.2096$. Moreover, maximum effective covert rates of $\bar{R}_{a,b}^* = 2.0585$ and 3.2223 are achievable at the target rates of $R_b = 2.88$ and 4.46 with the corresponding optimal outage probabilities of

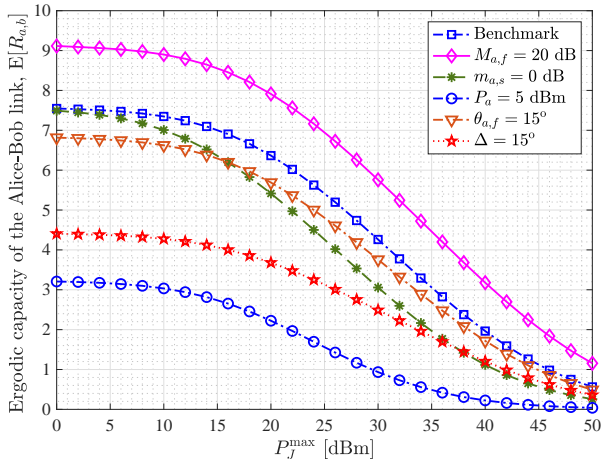


Fig. 4. The ergodic capacity $\mathbb{E}[R_{a,b}]$ of the Alice-Bob link for the benchmark scenario, corresponding to the parameters in Table II, and several other setups obtained by changing $M_{a,f}$, $m_{a,s}$, P_a , $\theta_{a,f}$, and Δ .

$P_{\text{out}}^{*AB} = 0.2853$ and 0.2775 for the scenarios of $P_a = 5$ dBm and $\theta_{a,s} = 15^\circ$, respectively. The optimal values of P_J^{max} for these two scenarios are $P_{J,\text{opt}}^{\text{max}} = 0.52$ dBm and 25.91 dBm, respectively. Although reducing $\theta_{a,s}$ to 15° does not directly impact the performance of the Alice-Bob link (e.g., the outage probability or ergodic capacity), it requires much stronger jamming signals with $P_{J,\text{opt}}^{\text{max}} = 25.91$ dBm to satisfy the covertness requirement which significantly degrades the performance compared to the benchmark scenario. On the other hand, the performance drop-off of the case $P_a = 5$ dBm is a direct consequence of the much lower transmit power used compared to the benchmark scenario though a much weaker jamming signal of $P_{J,\text{opt}}^{\text{max}} = 0.52$ dBm is enough to satisfy the covertness constraint.

The ergodic capacity $\mathbb{E}[R_{a,b}]$ of the Alice-Bob link is shown in Fig. 4 for the benchmark scenario, corresponding to the parameters in Table II. Moreover, the impact of several parameters is examined by changing each one while keeping the rest of the parameters as Table II. As expected, $\mathbb{E}[R_{a,b}]$ monotonically decreases by P_J^{max} . Moreover, higher values of $M_{a,f}$, P_a , and $\theta_{a,f}$ have positive impacts on the ergodic capacity while larger values of $m_{a,s}$ and Δ negatively impact $\mathbb{E}[R_{a,b}]$. It is worth mentioning at the end that mmWave links benefit from much larger bandwidths compared to RF links; hence, the results in Figs. 3 and 4 imply much higher data rates, in bits per second, compared to that of RF communication counterparts.

VII. CONCLUSIONS

In this paper, we investigated covert communication over mmWave links. We employed a dual-beam transmitter to simultaneously transmit the desired signal to the destination and propagate a jamming signal to degrade the warden's performance. We characterized Willie's detection error rate and the closed-form of its expected value from Alice's perspective. We then derived the closed-form expression for the outage probability of Alice-Bob link enabling us to formulate the optimal

achievable covert rates. We further obtained tractable forms for the ergodic capacity of Alice-Bob link involving only one-dimensional integrals that can be computed in closed forms for most ranges of the channel parameters. Moreover, we elucidated how the results can be extended to more practical scenarios, taking into account the uncertainty about Willie's location. We also highlighted several interesting directions for future research on covert mmWave communication. Through comprehensive numerical studies, we analyzed the behavior of the derived performance metrics with respect to variety of channel and system parameters. Our results demonstrated the advantages of covert mmWave communication compared to the RF counterpart, calling for further research on this novel area.

APPENDIX A

A USEFUL LEMMA FOR THE INTEGRATION OVER $\text{Ei}(\cdot)$

In [36, Lemma 1], a useful lemma is proved for the integral of $\int_{c_1}^{c_2} e^{bx} \text{Ei}(ax) dx$ with $c_1, c_2 > 0$, $a < 0$, and $b \in \mathbb{R}$ such that (s.t.) $a + b < 0$. In this appendix, we prove that the same result, with a slight change, can be applied to the case of $b = -a$, i.e., $a + b = 0$ (see, e.g., [37, Eq. (06.35.21.0014.01)]).

Lemma 7. For any $c_1, c_2 > 0$ and $a < 0$, we have

$$\int_{c_1}^{c_2} e^{-ax} \text{Ei}(ax) dx = \frac{1}{-a} \left[e^{-ac_2} \text{Ei}(ac_2) - e^{-ac_1} \text{Ei}(ac_1) - \ln(c_2/c_1) \right]. \quad (45)$$

Proof: Note based on [36, Lemma 1] that for $c_1, c_2 > 0$, $a < 0$, and $b \in \mathbb{R}$ s.t. $a + b < 0$, we have

$$\int_{c_1}^{c_2} e^{bx} \text{Ei}(ax) dx = \frac{1}{b} \left[e^{bt} \text{Ei}(at) - \text{Ei}([a + b]t) \right]_{c_1}^{c_2}, \quad (46)$$

where $f(t)|_{c_1}^{c_2} \triangleq f(c_2) - f(c_1)$ for the function $f(t)$. In the case of $b = -a$ per Lemma 7, the argument of the second exponential integral function $\text{Ei}([a + b]t)$ in (46) is zero. Based on [40, Eq. (1)], $\lim_{x \rightarrow 0} \text{Ei}(x) = \gamma + \ln|x|$, where $\gamma = 0.57721$ is the Euler's constant. Therefore, we can write $\text{Ei}([a + b]t)|_{c_1}^{c_2}$ for the case of $a = -b$ as

$$\text{Ei}([a + b]t)|_{c_1}^{c_2} = \lim_{x \rightarrow 0} \text{Ei}(xt)|_{c_1}^{c_2} = \lim_{x \rightarrow 0} \ln \left(\frac{|xc_2|}{|xc_1|} \right) = \ln \left(\frac{c_2}{c_1} \right). \quad (47)$$

This together with some similar arguments as the proof of [36, Lemma 1] completes the proof of Lemma 7. ■

REFERENCES

- [1] M. V. Jamali and H. Mahdaviyar, "Covert millimeter-wave communication via a dual-beam transmitter," in *Proc. IEEE Global Communications Conference (GLOBECOM), Waikoloa, HI, USA, Dec. 2019*, pp. 1–6.
- [2] B. A. Bash, D. Goeckel, and D. Towsley, "Limits of reliable communication with low probability of detection on AWGN channels," *IEEE J. Sel. Areas Commun.*, vol. 31, no. 9, pp. 1921–1930, 2013.
- [3] B. A. Bash, D. Goeckel, D. Towsley, and S. Guha, "Hiding information in noise: fundamental limits of covert wireless communication," *IEEE Commun. Mag.*, vol. 53, no. 12, pp. 26–31, 2015.
- [4] P. H. Che, M. Bakshi, and S. Jaggi, "Reliable deniable communication: Hiding messages in noise," in *IEEE Int. Symp. Inf. Theory (ISIT)*, 2013, pp. 2945–2949.

- [5] L. Wang, G. W. Wornell, and L. Zheng, "Fundamental limits of communication with low probability of detection," *IEEE Trans. Inf. Theory*, vol. 62, no. 6, pp. 3493–3503, 2016.
- [6] M. R. Bloch, "Covert communication over noisy channels: A resolvability perspective," *IEEE Trans. Inf. Theory*, vol. 62, pp. 2334–2354, 2016.
- [7] M. Tahmasbi and M. R. Bloch, "First-and second-order asymptotics in covert communication," *IEEE Trans. Inf. Theory*, vol. 65, no. 4, pp. 2190–2212, 2018.
- [8] K. S. K. Arumugam and M. R. Bloch, "Embedding covert information in broadcast communications," *IEEE Trans. Inf. Forensics Secur.*, vol. 14, no. 10, pp. 2787–2801, 2019.
- [9] —, "Covert communication over a K -user multiple-access channel," *IEEE Trans. Inf. Theory*, vol. 65, no. 11, pp. 7020–7044, 2019.
- [10] S. Lee, R. J. Baxley, M. A. Weitnauer, and B. Walkenhorst, "Achieving undetectable communication," *IEEE J. Sel. Topics Signal Process.*, vol. 9, no. 7, pp. 1195–1205, 2015.
- [11] D. Goeckel, B. Bash, S. Guha, and D. Towsley, "Covert communications when the warden does not know the background noise power," *IEEE Commun. Lett.*, vol. 20, no. 2, pp. 236–239, 2016.
- [12] B. A. Bash, D. Goeckel, and D. Towsley, "Covert communication gains from adversary's ignorance of transmission time," *IEEE Trans. Wireless Commun.*, vol. 15, no. 12, pp. 8394–8405, 2016.
- [13] J. Hu, S. Yan, X. Zhou, F. Shu, J. Li, and J. Wang, "Covert communication achieved by a greedy relay in wireless networks," *IEEE Trans. Wireless Commun.*, vol. 17, no. 7, pp. 4766–4779, 2018.
- [14] J. Wang, W. Tang, Q. Zhu, X. Li, H. Rao, and S. Li, "Covert communication with the help of relay and channel uncertainty," *IEEE Wireless Commun. Lett.*, vol. 8, no. 1, pp. 317–320, 2019.
- [15] K. Shahzad, X. Zhou, and S. Yan, "Covert communication in fading channels under channel uncertainty," in *IEEE VTC Spring*. IEEE, 2017, pp. 1–5.
- [16] K. Shahzad, X. Zhou, S. Yan, J. Hu, F. Shu, and J. Li, "Achieving covert wireless communications using a full-duplex receiver," *IEEE Trans. Wireless Commun.*, vol. 17, no. 12, pp. 8517–8530, 2018.
- [17] K. Shahzad, X. Zhou, and S. Yan, "Covert wireless communication in presence of a multi-antenna adversary and delay constraints," *IEEE Trans. Veh. Technol.*, vol. 68, no. 12, pp. 12432–12436, 2019.
- [18] J. Hu, S. Yan, X. Zhou, F. Shu, and J. Li, "Covert wireless communications with channel inversion power control in Rayleigh fading," *IEEE Trans. Veh. Technol.*, vol. 68, no. 12, pp. 12135–12149, 2019.
- [19] X. Zhou, S. Yan, J. Hu, J. Sun, J. Li, and F. Shu, "Joint optimization of a UAV's trajectory and transmit power for covert communications," *IEEE Trans. Signal Process.*, vol. 67, no. 16, pp. 4276–4290, 2019.
- [20] M. Forouzes, P. Azmi, A. Kuhestani, and P. L. Yeoh, "Covert communication and secure transmission over untrusted relaying networks in the presence of multiple wardens," *IEEE Trans. Commun.*, vol. 68, no. 6, pp. 3737–3749, 2020.
- [21] M. Forouzes, P. Azmi, N. Mokari, and D. Goeckel, "Covert communication using null space and 3D beamforming: Uncertainty of Willie's location information," *IEEE Trans. Veh. Technol.*, May 2020.
- [22] J. G. Andrews, T. Bai, M. N. Kulkarni, A. Alkhateeb, A. K. Gupta, and R. W. Heath, "Modeling and analyzing millimeter wave cellular systems," *IEEE Trans. Commun.*, vol. 65, no. 1, pp. 403–430, 2017.
- [23] S. L. Cotton, W. G. Scanlon, and B. K. Madahar, "Millimeter-wave soldier-to-soldier communications for covert battlefield operations," *IEEE Commun. Mag.*, vol. 47, no. 10, pp. 72–81, 2009.
- [24] J. Zhang, M. Li, S. Yan, C. Liu, X. Chen, M. Zhao, and P. Whiting, "Joint beam training and data transmission design for covert millimeter-wave communication," *arXiv preprint arXiv:2007.01513*, July 2020.
- [25] T. S. Rappaport, S. Sun, R. Mayzus, H. Zhao, Y. Azar, K. Wang, G. N. Wong, J. K. Schulz, M. Samimi, and F. Gutierrez, "Millimeter wave mobile communications for 5G cellular: It will work!" *IEEE access*, vol. 1, pp. 335–349, 2013.
- [26] M. Di Renzo, "Stochastic geometry modeling and analysis of multi-tier millimeter wave cellular networks," *IEEE Trans. Wireless Commun.*, vol. 14, no. 9, pp. 5038–5057, 2015.
- [27] T. Bai and R. W. Heath, "Coverage and rate analysis for millimeter-wave cellular networks," *IEEE Trans. Wireless Commun.*, vol. 14, no. 2, pp. 1100–1114, 2015.
- [28] M. K. Simon and M.-S. Alouini, *Digital communication over fading channels*. John Wiley & Sons, 2005, vol. 95.
- [29] M. Fereydoonian, M. V. Jamali, H. Hassani, and H. Mahdaviifar, "Channel coding at low capacity," in *IEEE Information Theory Workshop (ITW)*. IEEE, 2019, pp. 1–5.
- [30] M. V. Jamali and H. Mahdaviifar, "Massive coded-NOMA for low-capacity channels: A low-complexity recursive approach," *arXiv preprint arXiv:2006.06917*, 2020.
- [31] —, "A low-complexity recursive approach toward code-domain NOMA for massive communications," in *Proc. IEEE Global Communications Conference (GLOBECOM), Abu Dhabi, UAE, Dec. 2018*, pp. 1–6.
- [32] T. V. Sobers, B. A. Bash, S. Guha, D. Towsley, and D. Goeckel, "Covert communication in the presence of an uninformed jammer," *IEEE Trans. Wireless Commun.*, vol. 16, no. 9, pp. 6193–6206, 2017.
- [33] A. Browder, *Mathematical analysis: an introduction*. Springer Science & Business Media, 2012.
- [34] I. S. Gradshteyn and I. M. Ryzhik, *Table of integrals, series, and products*. Academic Press, 2007.
- [35] H. Alzer, "On some inequalities for the incomplete Gamma function," *Math. Comput.*, vol. 66, no. 218, pp. 771–778, 1997.
- [36] M. V. Jamali and H. Mahdaviifar, "Uplink non-orthogonal multiple access over mixed RF-FSO systems," *IEEE Trans. Wireless Commun.*, vol. 19, no. 5, pp. 3558–3574, 2020.
- [37] *The Mathematical Functions Site*. Accessed: June 24, 2020. [Online]. Available: <http://functions.wolfram.com>.
- [38] J. Zhang, X. Ge, Q. Li, M. Guizani, and Y. Zhang, "5G millimeter-wave antenna array: Design and challenges," *IEEE Wireless Commun.*, vol. 24, no. 2, pp. 106–112, 2016.
- [39] G. K. Karagiannidis and S. A. Kotsopoulos, "On the distribution of the weighted sum of L independent Rician and Nakagami envelopes in the presence of AWGN," *J. Commun. Netw.*, vol. 3, no. 2, pp. 1–8, 2001.
- [40] F. E. Harris, "Tables of the exponential integral $Ei(x)$," *Mathematical Tables and Other Aids to Computation*, vol. 11, no. 57, pp. 9–16, 1957.